ARMY RESEARCH LABORATORY

Liquid Core Structure of Evaporating Sprays at High Pressures - Flash X-Ray Studies

A. Birk
M. McQuaid
M. Gross

ARL-TR-901 December 1995

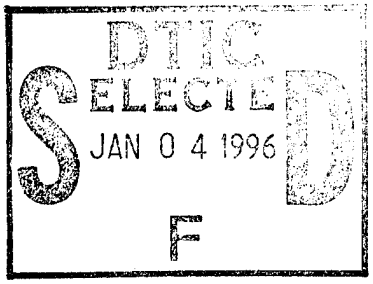

NOTICES

Destroy this report when it is no longer needed. DO NOT return it to the originator.

Additional copies of this report may be obtained from the National Technical Information Service, U.S. Department of Commerce, 5285 Port Royal Road, Springfield, VA 22161.

The findings of this report are not to be construed as an official Department of the Army position, unless so designated by other authorized documents.

The use of trade names or manufacturers' names in this report does not constitute indorsement of any commercial product.

REPORT DOCUMENTATION PAGE

Form Approved
OMB No. 0704-0188

1. AGENCY USE ONLY *(Leave blank)*	2. REPORT DATE	3. REPORT TYPE AND DATES COVERED
	December 1995	Final, May–Nov 1993

4. TITLE AND SUBTITLE
Liquid Core Structure of Evaporating Sprays at High Pressures - Flash X-Ray Studies

5. FUNDING NUMBERS
PR: 4G010534R30000

6. AUTHOR(S)
A. Birk, M. McQuaid, and M. Gross

7. PERFORMING ORGANIZATION NAME(S) AND ADDRESS(ES)
U.S. Army Research Laboratory
ATTN: AMSRL-WT-PA
Aberdeen Proving Ground, MD 21005-5066

8. PERFORMING ORGANIZATION REPORT NUMBER
ARL-TR-901

9. SPONSORING / MONITORING AGENCY NAME(S) AND ADDRESS(ES)

10. SPONSORING / MONITORING AGENCY REPORT NUMBER

11. SUPPLEMENTARY NOTES

12a. DISTRIBUTION / AVAILABILITY STATEMENT
Approved for public release; distribution is unlimited.

12b. DISTRIBUTION CODE

13. ABSTRACT *(Maximum 200 words)*

This report describes the development and application of flash x-ray radiography for studying the core structure of atomizing jets at high temperatures (to 2,300 K) and pressures (1.4–13.8 MPa). Methyl iodide (CH_3I) was injected at approximately 75 m/s through a 1-mm-circular orifice into (hot) nitrogen or the post-combustion products of an H_2/Air/Ar mixture. Similar experiments involving injections at 40 m/s through thin, annular orifices were also conducted. Radiographs which resolve core details to less than 0.1 mm were achieved. We observed that the core structure is strongly affected by heat transfer under these conditions. The cores of circular jets were found to develop helical structure whose pitch angle decreased with axial distance from the orifice. As expected, the core penetration distance decreased with increase in ambient gas density. A surprising result was that for the same global ambient gas density, the length of evaporating cores decreased with increase in ambient pressure (and temperature) up to a "critical" value, then increased with further rise in pressure. The minimum corresponds to a transition to a pressure and temperature regime above the *thermodynamic* critical point of the liquid.

14. SUBJECT TERMS
atomization, heat transfer, liquid propellants, radiography

15. NUMBER OF PAGES
25

16. PRICE CODE

17. SECURITY CLASSIFICATION OF REPORT	18. SECURITY CLASSIFICATION OF THIS PAGE	19. SECURITY CLASSIFICATION OF ABSTRACT	20. LIMITATION OF ABSTRACT
UNCLASSIFIED	UNCLASSIFIED	UNCLASSIFIED	UL

INTENTIONALLY LEFT BLANK.

TABLE OF CONTENTS

		Page
	LIST OF FIGURES	v
1.	INTRODUCTION	1
2.	DESIGN CONSIDERATIONS FOR FLASH X-RAY EXPERIMENTS	2
3.	EXPERIMENTAL SETUP AND OPERATION	6
4.	IMAGE PROCESSING	10
5.	TEST MATRIX	11
6.	RESULTS	11
6.1	General Observations	11
6.2	Physical Interpretation	17
7.	PRACTICAL IMPLICATIONS	18
8.	CONCLUSIONS	18
9.	REFERENCES	21
	DISTRIBUTION LIST	23

INTENTIONALLY LEFT BLANK.

LIST OF FIGURES

Figure		Page
1.	Experimental setup	7
2.	Test chamber detail	8
3.	Typical test data (test series C)	9
4.	Visual and x-ray records of evaporating and nonevaporating sprays in test series A	13
5.	X-ray records of jets in test series B–D: (a) nonevaporating, (b) subcritical evaporation, (c) transcritical, and (d) supercritical	14
6.	Visual and x-ray records of annular jets	15

INTENTIONALLY LEFT BLANK.

1. INTRODUCTION

Despite perennial research in pressure-atomized liquid jets, the ability to characterize the core structure of such jets has been extremely limited. This limitation arises from the inability to observe such structures using standard visualization techniques. For "atomizing" jets (i.e., jets that begin to diverge immediately at the nozzle exit), the liquid core is shrouded by an optically dense cloud of droplets. Two experimental techniques have been developed to overcome this obstacle: an electric grid method (Chehroudi et al. 1985) and flash x-ray photography (Baev et al. 1986; Warken and Krehl 1990). The former identifies the length of the core penetration when the core creates an electrical path between the nozzle and a downstream electrical probe. Despite the success reported in obtaining data with this technique, it does not provide the overall core structure and the measurement is intrusive. Flash x-ray photography takes advantage of the fact that x-rays, defined as radiation with wavelengths in the range 0.1 to 10 nm, are only scattered at the molecular level following absorption, not at interfaces. Thus, radiography provides a shadowgraph corresponding to molecular density. Despite the promise of this technique and its advantages over the electric grid method, only a few studies have been reported and these studies have dealt primarily with circular jets under nonevaporating conditions.

This report describes the implementation of the flash x-ray technique for studying the core structure of atomizing jets at high temperatures and pressures. This work stems from our efforts to resolve issues related to the development of liquid propellant gun technology (Morrison, Knapton, and Bulman 1988). The current technology is based on regeneratively injecting a liquid monopropellant into the combustion chamber. The combustion intensities in such devices are extremely high and large-scale pressure fluctuations have been observed in nearly all such gun designs tested to date. The pressure fluctuations are presumably associated with the unstable combustion of unreacted liquid in the chamber. Though there is no direct experimental evidence, it is considered that little liquid exists beyond the jet's core. If this is the case, then the core represents the bulk of the unreacted liquid and its distribution in the chamber. Thus, there may be a correlation between the core structure (dynamics) and the observed pressure fluctuations. Beyond this application, the current study has ramifications for diesel and liquid rocket engines, both of which involve injection into high temperature and pressure environments. In recent years, interest in improving the performance of such systems has led to designs in which the liquid traverses its critical point prior to combustion. There is a tangible need for better data on such systems. For example, theory and experimental data obtained with the electric grid method suggests the core penetration distance (L_C) can be predicted via the equation,

$$L_C = C_o d_o \left(\rho_L/\rho_G\right)^{1/2} , \quad (1)$$

where C_o is a constant, d_o is the nozzle diameter, and ρ_L and ρ_G are the liquid and gas densities, respectively. However, numerical simulations of diesel engine spray combustion underestimate the experimentally observed spray penetration distance (Gonzalez and Reitz 1991).

The implementation of flash radiography for characterizing the core structure of atomizing jets evaporating at high temperatures and pressures is challenging because the injection must be radiographed through chamber windows that will not fail under such conditions. The chemical composition and thickness of windows having the required physical strength can significantly attenuate the x-ray beam intensity. Also, the injection orifice must be relatively small so that the entire core can be observed in a reasonably sized pressure vessel. Both of these requirements limit the contrast achievable in a single flash x-ray image. We have overcome these difficulties through judicious experimental design. Reported here are the results obtained from experiments where methyl iodide (CH_3I) was injected at approximately 75 m/s through a circular orifice into either (hot) nitrogen or the post-combustion products of H_2/Air/Argon mixtures. The results from similar tests involving CH_3I injections at 40 m/s through annular orifices are also presented. Methyl iodide, an unusual choice for such a study, has a combination of desirable properties: namely, a high x-ray absorption cross section, well-characterized physical parameters, and a critical point which can be exceeded in our test chamber. In addition to flash x-ray data, jet images based on visible light scattering were obtained for injections into nitrogen. The results are analyzed in terms of variation in gas density, temperature, and pressure.

2. DESIGN CONSIDERATIONS FOR FLASH X-RAY EXPERIMENTS

The two most important parameters controlling the ability to resolve details in a flash x-ray image are the contrast and penumbra. The "intrinsic" contrast (C) is defined in terms of differences in transmitted beam intensity for different thicknesses of the same material. The intrinsic contrast is rendered experimentally by exposing a detector. (In this work, the detector is a film-intensifying screen combination.) This produces a monochrome image (transparency) whose optical densities correspond to transmitted intensities. Penumbra is an intrinsic "unsharpness" due to the fact that the x-ray beam diverges from the source (i.e., the beam's rays are not parallel as they pass through the object). Each of these considerations is discussed in the following sections. This discussion is based on Krehl and Warken

(1990) and a Hewlett-Packard Technical Bulletin (1973) and they are recommended for readers interested in a more complete discussion of these aspects of radiography.

For a monochromatic beam with wavelength λ, passing through a sample of thickness x, the ratio of transmitted ($I_t[\lambda]$) to incident [$I_i(\lambda)$] intensity is given by

$$T(\lambda) = I_t(\lambda)/I_i(\lambda) = \exp[-\mu(\lambda)x] , \tag{2}$$

where $\mu(\lambda)$ is the linear absorption cross section of the sample, and $I_i(\lambda)$ is equal to

$$I_i(\lambda) = \left[\prod_n T_n(\lambda)\right] I_S(\lambda) , \tag{3}$$

where $I_S(\lambda)$ is the output of the x-ray source and $T_n(\lambda)$ is the transmissivity through non-object elements in the path. Neglecting, for the moment, film response vs. exposure considerations, it can be shown that the contrast [$C(\lambda)$] between two objects (n and n + 1) of the same material is given by

$$C(\lambda) \equiv \left[I_n(\lambda) - I_{n+1}(\lambda)/I_n(\lambda)\right] = 1 - \exp[-\mu(\lambda)\Delta x] , \tag{4}$$

where Δx is the difference in thickness of objects n and n + 1. The transmission properties of uniformly thick, nonobject elements (such as windows) are not important at this level of analysis. For a polychromatic source, the contrast will be a weighted average of the intensity distribution,

$$C = 1 - \int I_i(\lambda) \exp[-\mu(\lambda)\Delta x] \, d\lambda \; / \; \int I_i(\lambda) \, d\lambda . \tag{5}$$

Thus, designing an experiment to optimize the intrinsic contrast requires a knowledge of the spectral output of the x-ray source, the transmissivity characteristics of the object and nonobject elements, and the wavelength dependence of the sample's absorption cross section.

The transmissivity of nonobject elements in the path is also important when film response is considered. For a given film, optimal rendering of the intrinsic contrast depends primarily on maximizing the change in the optical density [OD ≡ log (I_i / I_t)] per change in x-ray intensity incident on the film (I); i.e., dOD(I) / dI. (Note, that in the definition of OD, the parameters I_i and I_t are incident and transmitted intensities associated with scanning the transparency. They should not be confused with incident and transmitted x-ray intensities associated with exposing the film.) In general, there will be an optimal incident x-ray intensity (exposure) range which maximizes dOD(I) / dI.

The penumbra (y) is a function of the object-to-film distance (r_{of}), the x-ray tube-to-film distance (r_{sf}), and the focal diameter of the x-ray source (D_x),

$$y = D_x \, r_{of} \, / \, (r_{sf} - r_{of}) \, . \tag{6}$$

The focal diameter is fixed by the source hardware, but penumbra can be minimized by decreasing r_{of} and increasing r_{sf}.

Equations 3, 4, and 5, coupled with film response and penumbra considerations, guided our effort to design a system where the details of the liquid core structure could be resolved down to 0.1 mm. The flash x-ray unit available to us was a standard 150-KV Hewlett-Packard system. The flash duration of this system is sufficiently short (50 to 70 ns) to freeze the jet motion. Several different x-ray target/window (tube material) configurations are available for this system and these configurations determine $I_S(\lambda)$. Since we were interested in resolving the details of "thin" objects—and x-ray absorption cross sections generally increase with decreasing photon energy—a spectrum of "soft" (20 keV) to "medium" (20 to 50 keV) x-ray output was desired. This dictated the use of a beryllium (vs. aluminum) windowed tube and a tungsten target. The tungsten target has an emission spectrum heavily weighted with "very soft" (< 10 keV) and medium x-rays. In choosing test chamber windows and a liquid to inject, absorption cross section was the primary consideration. Since absorption cross sections in the x-ray energy range tend to increase with increasing atomic number, we searched for (1) liquids with a high density of high (≥ 50) atomic number constituents and (2) polymers with low atomic number constituents for windows. The search for an appropriate liquid centered on iodine (atomic number = 53) containing molecules. CH_3I was selected because it had the desirable properties of being a liquid at room conditions, a thermodynamic critical point which could be exceeded in our test chamber, and well-characterized physical properties (see Table 1). Polycarbonate (Lexan™, $[C_{16}H_{14}O_3)_n]$ and polypropylene $[(C_3H_6)_n]$

Table 1. Test Liquid (CH_3I) Properties[a]

ρ_L (g/cm^3)	μ_L (g/cm·s)	σ_L (g/s^2)	P_{crit} (MPa)	T_{crit} (K)	Oh[b]
2.279	0.005	25	7.366	528	0.002

[a] From Handbook of Chemistry and Physics. (Near room temperature).
[b] Ohnsorge number = $\mu_L/(\rho_L\sigma_L d_0)^{1/2}$ (given for d_0 = 0.1 cm).

were selected as window materials based on their ready availability and previous experience with such windows at the pressures of these experiments. These choices determined the basic experimental configuration, and all other considerations were based on achieving the best results with this hardware and liquid.

To render the x-ray image, a number of film-intensifying screen combinations were tested. The combination which yielded the highest OD/exposure for the basic experimental configuration was NDT 57 (Dupont) film with a Trimax 8 (3M) intensifying screen. For this combination, background optical densities of approximately 3.5 were achievable. (Note that background areas correspond to the highest optical densities in the image.) Such exposures would have maximized the dynamic range of gray levels in the image. Unfortunately, our optical scanner was unable to reliably digitize transparencies with OD ≥ 2.5. Therefore, experimental parameters were adjusted to produce background optical densities less than this value—with an attendant decrease in dynamic range.

To minimize penumbra, the film-to-jet distance was made as small as possible. The minimum object-to-film distance (r_{of} = 4.4 cm) was imposed by the dimensions of the test chamber. The x-ray tube-to-film distance (r_{sf} = 42.4 mm) was a compromise between (1) penumbra considerations, which are reduced with increasing r_{sf} (equation 6); and (2) achieving the desired optical densities, which fall off as r_{sf}^2. It was found that jet details with good signal-to-noise ratio were obtained when image optical densities fell in the range OD = 0.9 to 2. Substitution of these r_{sf} and r_{of} values into equation 6 yields a penumbra value of 0.31 mm. Since the actual resolution is typically five times better than the penumbra, the goal of resolving core structure details to less than 0.1 mm was achieved.

3. EXPERIMENTAL SETUP AND OPERATION

The experimental setup and details of the major components are shown in Figures 1 and 2. The test chamber is a 20.3-cm-long steel cylinder with a 5.72-cm I.D. The chamber contains two pairs of opposing ports at 90° to each other. One pair of ports contains windows (9.8 cm × 3.5 cm) which provide access for radiography and photography. The front window of this pair, through which it was desired to have visible access, was made of 1.9–2.5-cm-thick polycarbonate (Lexan™). Lexan™ is visually transparent and has a relatively high strength vs. x-ray absorption cross-section ratio. Since visible access was not required through the rear port, it was fitted with a polypropylene window. (Polypropylene is more resilient than Lexan™.) The radiographic film and intensifying screens were encased in a thin, light-tight plastic envelope and mounted between the polypropylene window and a Lexan™ flange as shown in Figure 2. This assembly was clamped together by the port's mounting bolts. A rubber pad was placed between the Lexan™ flange and the film pack to uniformly distribute the pressure on the intensifying screens. The other ports included (1) a clear Lexan™ window (7 cm × 1.9 cm), through which the jet could be illuminated with visible light for standard photography; and (2) a spark plug, gas port, and the thermocouple port (not shown).

Two methods were employed for providing high-temperature and pressure ambient gas. The first method (test series A) involved delivering nitrogen to the test chamber from a high-pressure gas reservoir via a particle bed heater (Birk and McQuaid 1993). The second method (test series B–E) involved igniting a pressurized stoichiometric mixture of H_2/Air/Ar in the test chamber with an automotive-type spark plug. (Argon was used in the mixture to facilitate ignition and prevent detonation.) The temperature (T_C) and pressure (P_C) of the resulting combustion products reached near adiabatic limits in approximately 5 ms, then dropped due to heat losses to the chamber walls (Figure 3). By controlling the injection timing with respect to ignition, different (P_C, T_C) values for the same ambient gas density (ρ_G) could be produced.

Chamber (P_C) pressure was measured with a piezoelectric pressure transducer (Kistler, Model 601B1). Measurement of the test chamber temperature depended on the method used to generate the ambient gas conditions. In test series A, where the chamber was loaded with nitrogen through the particle bed heater, the gas temperature (T_C) was recorded using an exposed 0.05-mm chromel-alumel thermocouple. In test series B–E, where the stoichiometric H_2/Air/Ar mixture was ignited, T_C was calculated from the measured P_C at the time of the x-ray pulse. The calculation is based on computing the adiabatic pressure (P_{CA})

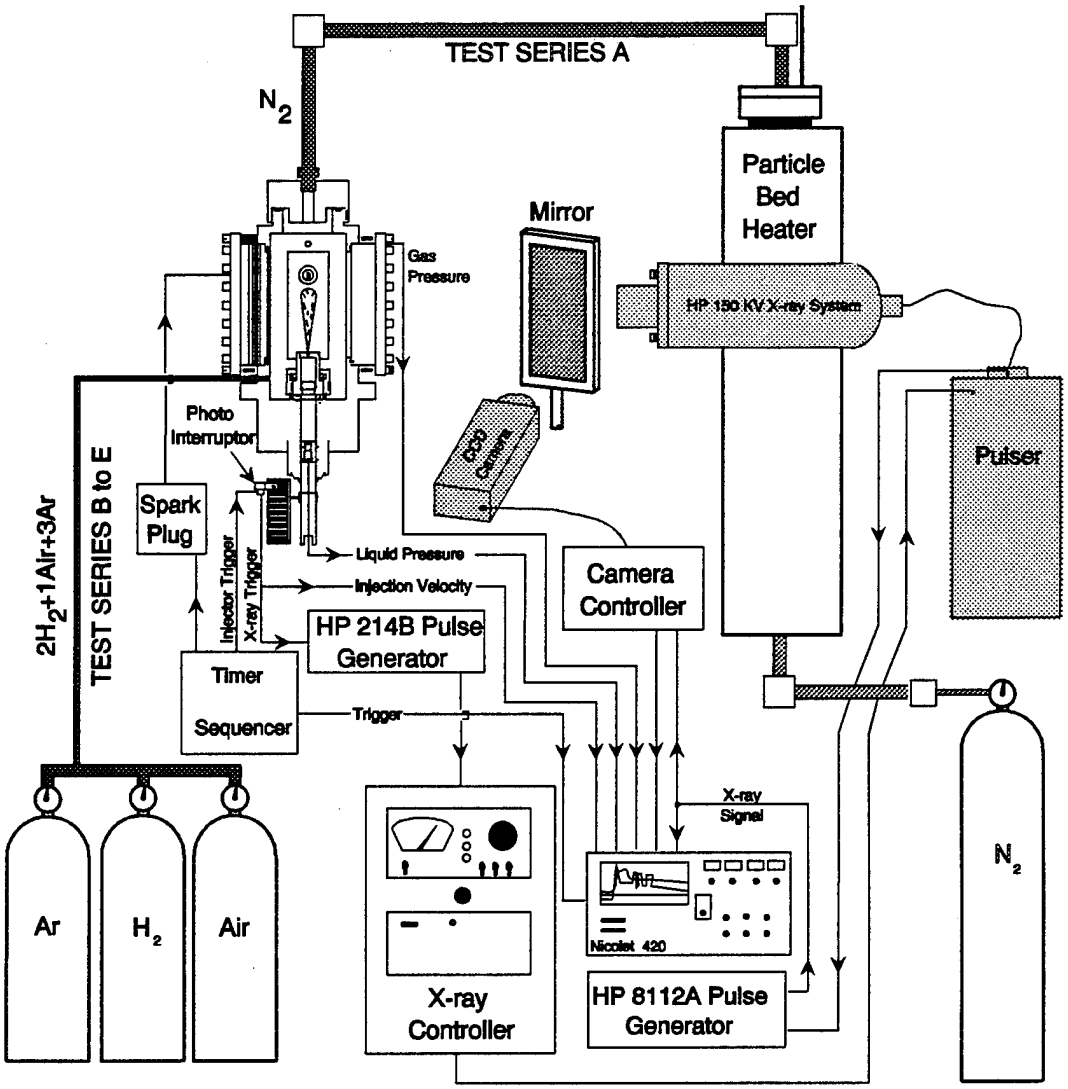

Figure 1. Experimental setup.

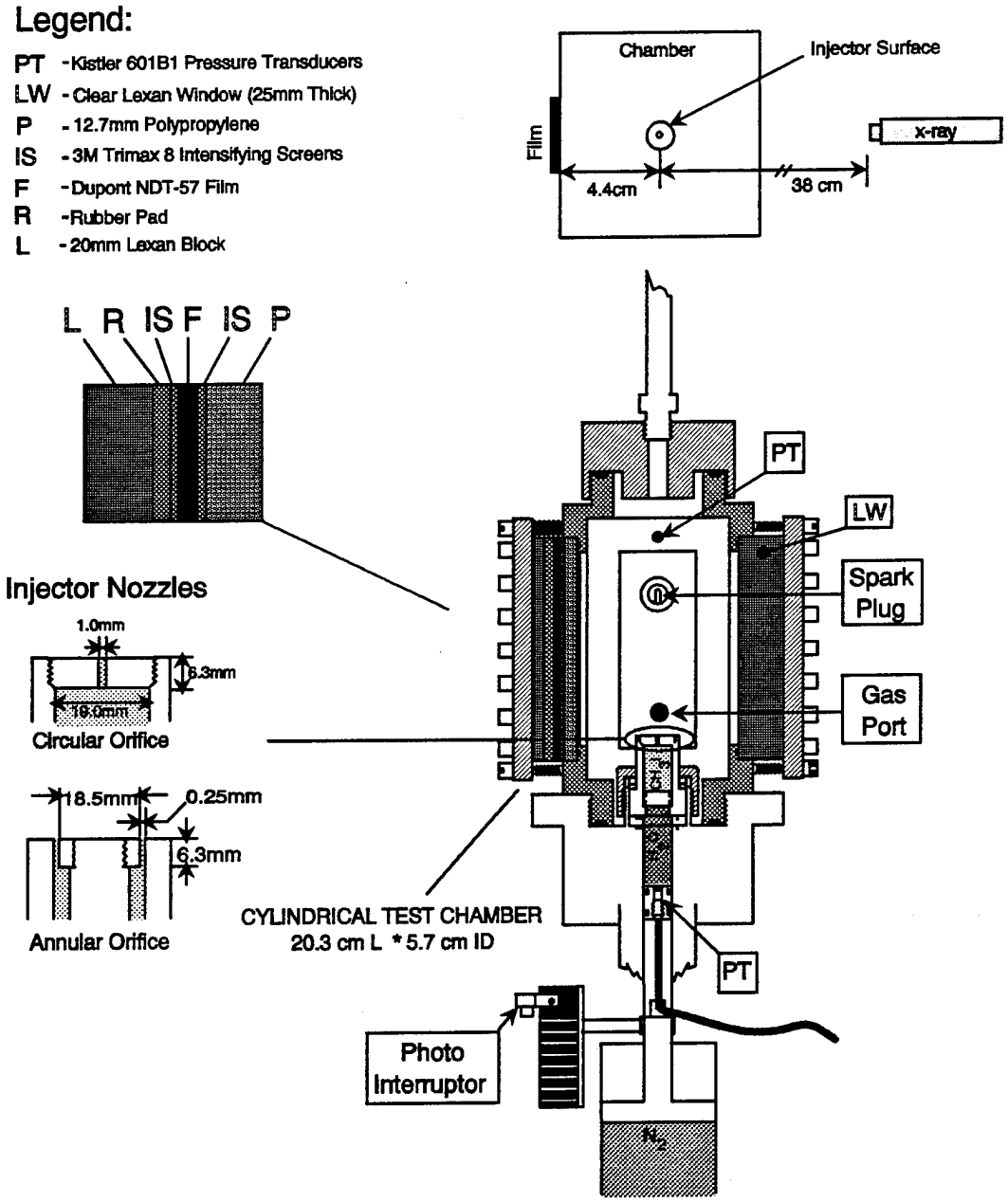

Figure 2. Test chamber detail.

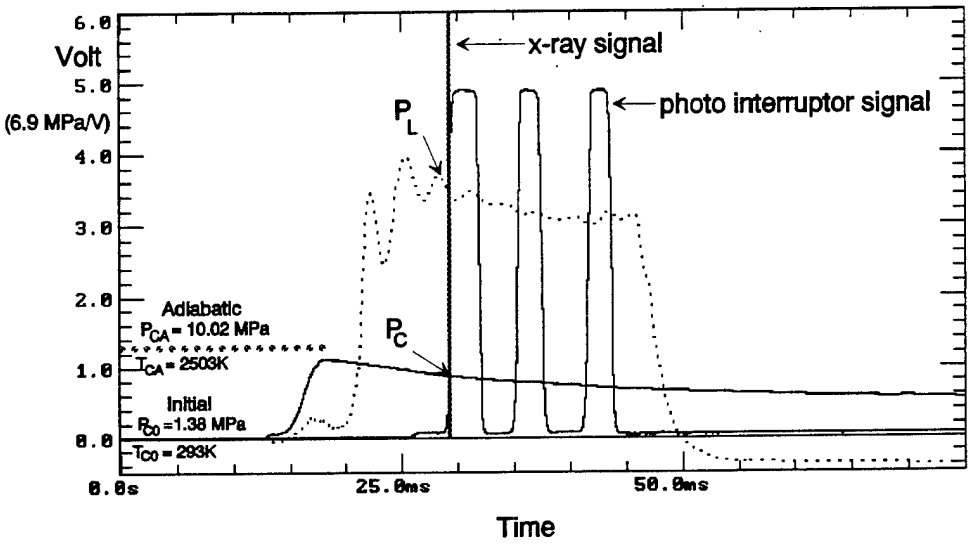

Figure 3. Typical test data (test series C).

and temperature (T_{CA}) for the mixture using the Blake thermodynamics code (Freedman 1982). Since the chamber volume is constant, and approximately 9 mol of gas products are generated for every 10 mol of reactant, T_C can be calculated from the initial gas temperature (T_{C0}) and pressure (P_{C0}), and a modified equation of state for the gas, viz.,

$$T_C = (10/9) \times \left[(P_C \times T_{C0})/P_{C0}\right] \times \left[1 + K\,(P_C - P_{C0})/(P_{CA} - P_{C0})\right], \qquad (7)$$

where K is a correction factor that scales T_C over the range T_{C0} to T_{CA} for P_C between P_{C0} and P_{CA}. (K = 0.058, 0.057, 0.055 for [P_{C0}, P_{CA}] = [1.379, 10.02]; [1.724, 12.56]; [2.069, 15.12] MPa and [T_{C0}, T_{CA}] = [293, 2503]; [293, 2507]; [293, 2509] K, respectively.) Typically, the maximum P_C obtained was 90% of P_{CA}.

Methyl iodide was injected vertically upward into the test chamber via an injector in the base of the test chamber. The injector is pneumatically actuated and utilizes hydraulic-pressure amplification to drive the liquid (Birk and Reeves 1987). The pressure exerted on the liquid during the injection was measured

with a piezoelectric pressure transducer (Kistler, Model 601B1). A photo-interrupter (based on a GE H11A2 photodiode) was arranged so that a comb-like mask attached to the injector's pushrod passed through it. The (square wave) signal from this configuration was used to monitor the injection velocity (Figure 3) and trigger the flash x-ray unit. An output signal associated with the triggering of the x-ray tube was recorded in order to ascertain the injection parameters at the time the x-ray image was taken.

In addition to the flash x-ray photographs, corresponding images based on visible light scattering were obtained with an intensified-CCD camera in test series A. (In test series C–E, the intense radiation from the hot gas products washed out the camera images.) The camera employed (EEV) has a 578 × 244-pixel array and was equipped with a TV zoom lens (Fujinon, Model C6x17.5B). To obtain images that froze the fluid motion, the f-stop of the lens was set to 1.8, and an exposure setting of 1 μs was chosen. The camera's intensifier gain was set to maximize the image's intensity range at these settings. The gain setting (approximately 2.5 out of 10) was established by trial and error during preliminary testing. (Note that exposure is an exponentially increasing function of the gain.)

To record the same field of view as the x-ray image, the camera viewed the injection via a 3-mm-thick mirror (aluminum-coated glass) in the path of the x-ray beam and at 45° to its axis. Preliminary testing showed that the mirror did not degrade the x-ray image. The camera was also rotated 90° to its normal (horizontal) orientation to take best advantage of the CCD element aspect ratio. The effective resolution of this configuration was approximately 0.2 mm/pixel. The camera was triggered simultaneously with the flash x-ray pulse, and an output corresponding to exposure onset and duration was recorded. Thus, the jet core (recorded in the x-ray image) and the spray envelope (recorded via the camera) can be superposed to establish the relationship between the two.

4. IMAGE PROCESSING

The x-ray film exposed during an experiment was developed with an automatic processor (DuPont, Model NDT 100) at normal settings. The jet appears as light shades of bluish-gray on a dark-gray background in the resulting transparencies. The dynamic range of the optical densities in the transparencies typically ranged from 0.5 to 2.5. This corresponds to a (digital) gray-level range of about 100. Digital images of these transparencies were obtained with a PC-based optical scanner (Artiscan, Model 8000C). The transparencies were well reproduced at a scanner resolution of 200 pixels/cm. Scan control and image processing was done with Aldus Photostyler. All digitized

images were handled in an 8-bit gray level format (TIF). To maximize the dynamic range in the digital recording, the scanner's exposure was set to yield a maximum gray level value for the core adjacent to the injector while maintaining background values near 0 ("black"). These images were then processed to yield images with 256 gray levels (0–255). This pseudoexpansion of the dynamic range facilitated image analysis and reproduction.

In the CCD camera images, the jet also appears as light shades of gray on a dark-gray background. The digital image created by the camera was converted to a video signal and recorded on videotape. It was then digitized with a PC-based frame-grabber. Direct transfer of the digital image to a computer is possible, but this procedure proved unreliable. The difficulty was presumably due to the noisy electromagnetic environment created by the experiment.

5. TEST MATRIX

The test parameters are summarized in Table 2. The present work is restricted to the study of effects of variation in ambient gas temperatures, pressures, and densities. The annular jets had smaller thicknesses and velocities than the full cone jets due to experimental constraints. In all tests, the radiograph was taken after the injection pressure reached steady state. Because only one radiograph was obtained per test, a certain redundancy was incorporated into the test matrix to statistically validate the results. A limited number of tests with 0.5-mm and 2-mm jets were also conducted. These tests provided a measure of liquid density distribution vs. gray level. They also indicated that the experimental trends observed with the 1-mm jets span this jet diameter range. As expected, the core's penetration distance scaled with jet thickness.

6. RESULTS

6.1 General Observations. Figures 4, 5, and 6 represent typical flash x-ray and CCD camera images obtained in the experiments. They demonstrate the success of radiography in revealing the liquid core structure under all ambient conditions. Furthermore, they show that the core is not a well-defined structure whose diameter linearly diminishes with downstream distance. Rather it is a zone in the jet whose liquid or liquid/vapor concentration per unit volume is much higher than that of the overall spray. Many of the experiments show accumulation of CH_3I liquid/vapor far downstream. This is expected since it is a closed chamber. We estimate that an x-ray absorption path length through 0.1-mm CH_3I in liquid form is equivalent to a path length of 3 to 10 mm in the accumulated gas.

Table 2. Test Parameters[g, h]

Series (no. of tests[a])	ρ_G (g/cm^3)	P_C (MPa)	T_C (K)	ρ_L/ρ_G	μ_0 (m/s)	$Re_G \times 10^{-4}$	L_C (cm) (calc.)
A[b]							
(3,2)	0.074	6.48	293	32.1	55–94	19.2–32.8	6.23
(8,2)	0.074	13.79	623	32.1	55–89	12.8–20.7	6.23
B[c]							
(2,2)	0.0141	1.38	293	161.6	74	4.9	14.0
	0.0141	1.38	293	161.6	95	7.3	14.0
C[d]							
(11,1)	0.0141	4.9–9.0	1,187–2,225	161.6	75–87	1.3–2.3	14.0
D[e]							
(3,0)	0.0176	8.0	1,561	129.5	75	2.0	12.5
	0.0176	10.28	2,028	129.5	88	2.2	12.5
	0.0176	11.45	2,273	129.5	77	1.5	12.5
E[f]							
(2,0)	0.0211	12.1	1,978	108	85	2.2	11.4
	0.0211	12.88	2,119	108	77	1.9	11.4

[a] (circular jet, annular jet).
[b] Injection into N_2 (u_0 = 38–44 m/s for annular jets).
[c] Injection into $2H_2 + 10_2 + 4N_2 + 3Ar$.
[d] Injection into the combustion products ($2H_20 + 4N_2 + 3Ar$) of test series B gas.
[e] Same as C, but with precombustion pressure of 1.724 MPa.
[f] Same as C, but with precombustion pressure of 2.069 MPa.
[g] $Re_G = \rho_G u_0 d_0/\mu_G$ (jet Reynolds number in the gas).
[h] Net injection pressures (P_L-P_C) ranged from 8.2 MPa to 26.2 MPa for circular jets, and 4.8 to 7.6 MPa for annular jets. Discharge coefficient values range from 0.58 to 0.68. Liquid Reynolds number ($Re_L = \rho_L u_0 d_0/\mu_L$) for the circular jets range from 2.5×10^4 to $3. \times 10^4$.

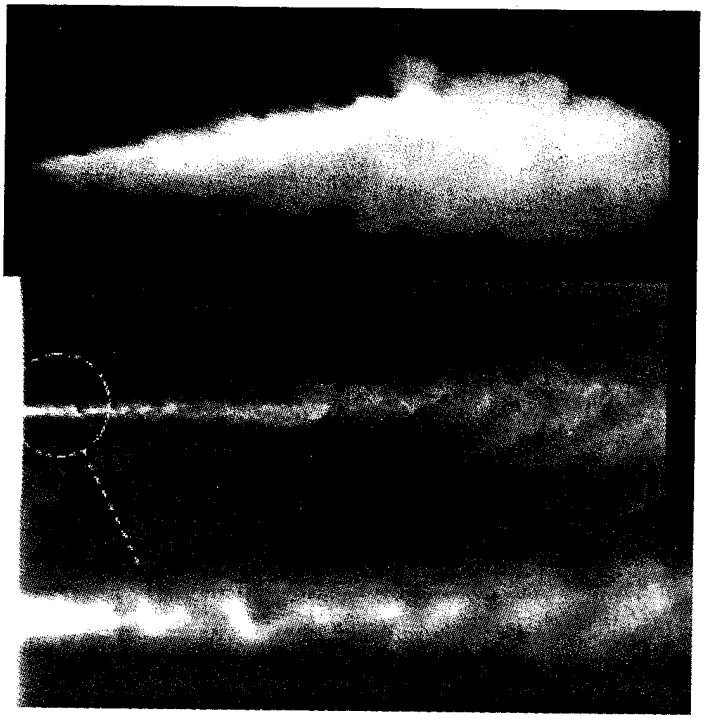

4a. Nonevaporating
u_0 = 90 m/s
P_C = 6.48 MPa
T_C = 293 K
ρ_L/ρ_G = 32.1

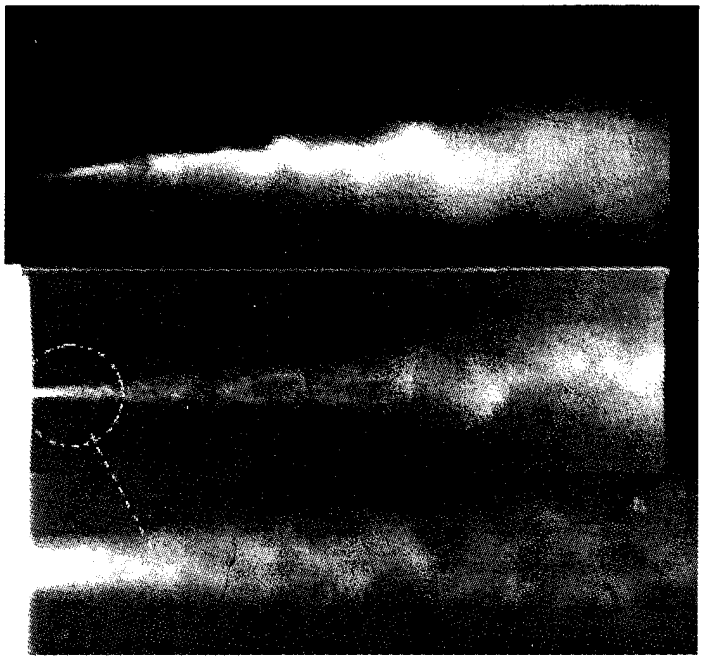

4b. Evaporating
u_0 = 68 m/s
P_C = 13.79 MPa
T_C = 623 K
ρ_L/ρ_G = 32.1

Figure 4. Visual and x-ray records of evaporating and nonevaporating sprays in test series A.

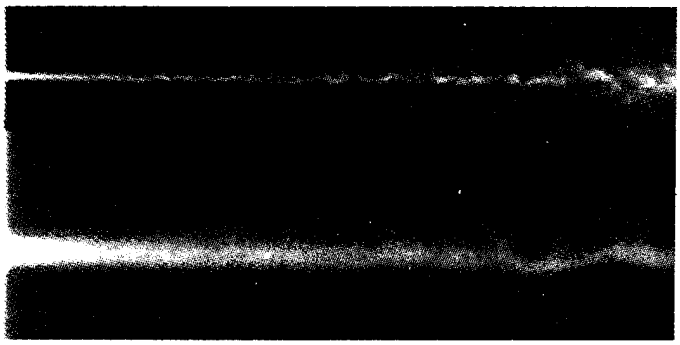

5a.
u_0 = 74 m/s
P_C = 1.38 MPa
T_C = 293 K
ρ_L/ρ_G = 161.6

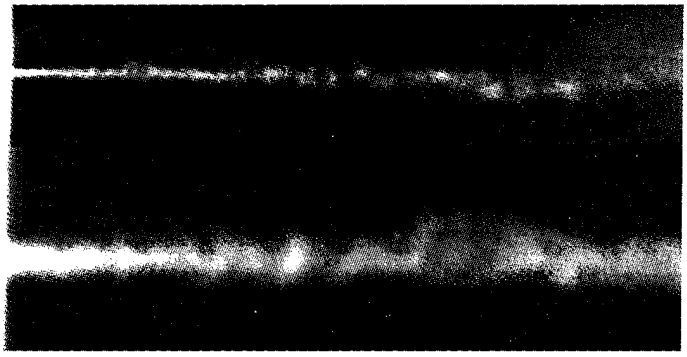

5b.
u_0 = 86 m/s
P_C = 6.48 MPa
T_C = 1,581 K
ρ_L/ρ_G = 161.6

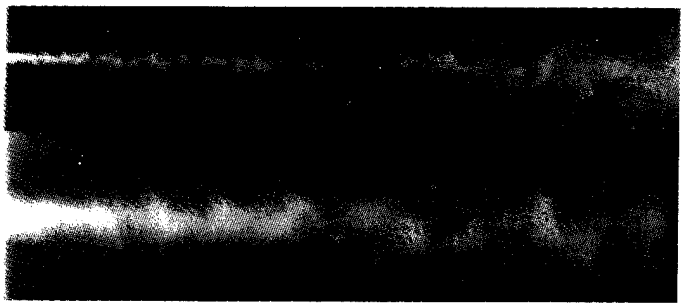

5c.
u_0 = 86 m/s
P_C = 8.97 MPa
T_C = 2,225 K
ρ_L/ρ_G = 161.6

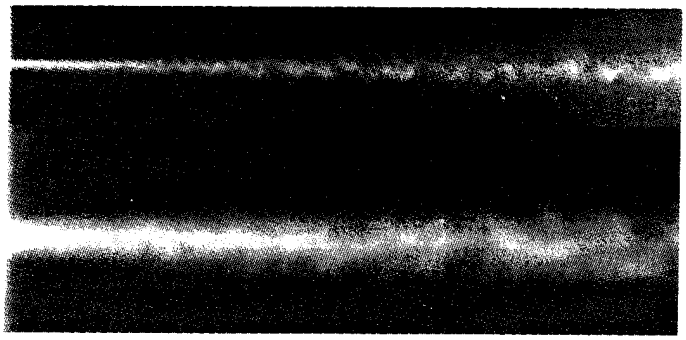

5d.
u_0 = 88 m/s
P_C = 10.28 MPa
T_C = 2,028 K
ρ_L/ρ_G = 129.5

Figure 5. X-ray records of jets in test series B–D: (a) nonevaporating, (b) subcritical evaporation, (c) transcritical, and (d) supercritical.

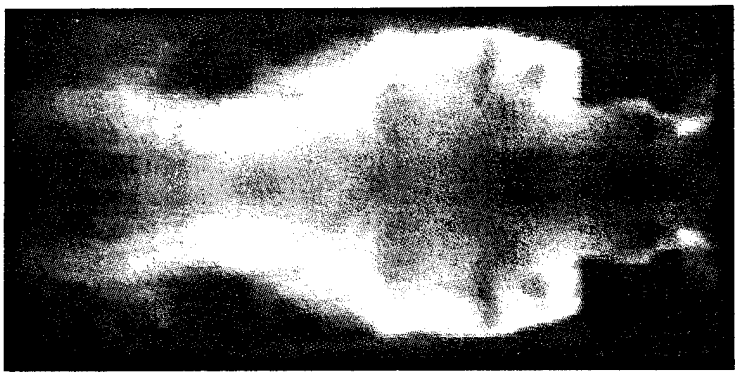

6a.
Visual record of top half of 6b. (Image is processed. See text for discussion.)

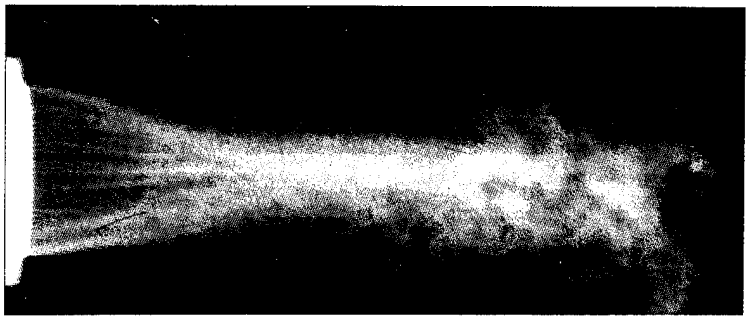

6b.
u_0 = 43 m/s
P_C = 6.48 MPa
T_C = 293 k
ρ_L/ρ_G = 32.1

6c.
u_0 = 38 m/s
P_C = 13.79 MPa
T_C = 623 K
ρ_L/ρ_G = 32.1

Figure 6. Visual and x-ray records of annular jets.

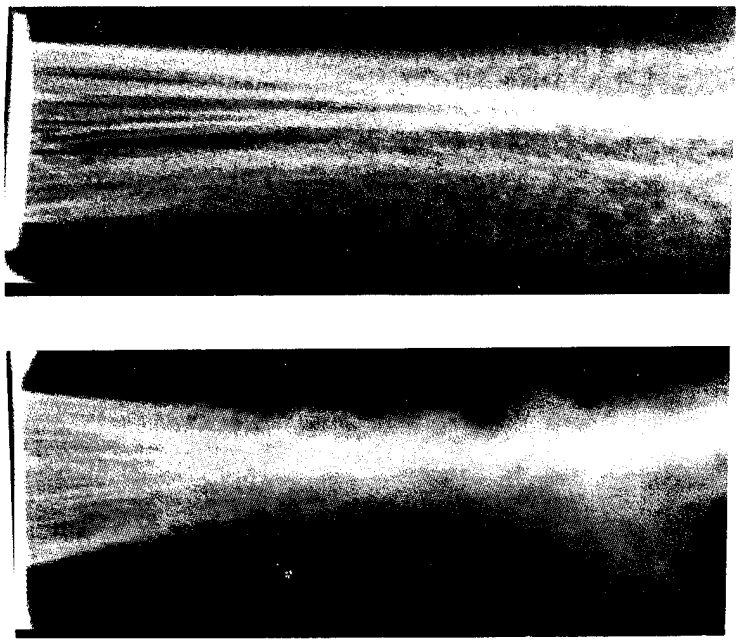

6d.
u_0 = 40 m/s
P_C = 1.38 MPa
T_C = 293 K
ρ_L/ρ_G = 161.6

6e.
u_0 = 38 m/s
P_C = 8.83 MPa
T_C = 2,189 K
ρ_L/ρ_G = 161.6

Figure 6. Visual and x-ray records of annular jets (continued).

Figures 4 and 5 show that within a few jet diameters, the cores of the full-cone sprays become helical, with average pitch decreasing with travel downstream. This is also noticeable in the CCD-imaged photograph of the evaporating jet (Figure 4b). In a prior test program (Birk, McQuaid, and Bliesener 1992), we observed intermittent helical structure in the high-speed cinemagraphic records of ethanol jets injected into ambient gas at a temperature and pressure above the critical point of ethanol.

The core structures of evaporating jets differ greatly from those of nonevaporating jets. The core penetration distance decreases with an increase in ambient gas pressure and density as expected (Table 2). Surprisingly, however, when sprays evaporated at temperature and pressure above the critical point of CH_3I, but at the same global-ambient gas density, core penetration increased with pressure (in the range tested). (It should be noted that the actual critical pressure in our tests will be higher than that of pure CH_3I because the ambient gas, which dissolves into CH_3I, has a large fraction of H_20 with a critical point of [647 K, 21.5 MPa].)

Figure 6 shows the results from a test with an annular configuration. (Note: In Figure 6a, only one boundary of the jet was illuminated and recorded. The lit boundary was flipped vertically and appended to the original to produce the image.) The core emerges from the injection port as a cylindrical shell composed of streamwise ligaments. The shell tends to collapse inward after a short travel (1–2 shell diameters), and more quickly at higher ambient pressures and temperatures. When magnified, many ligaments exhibit the helical structure observed in the cores of the full cone sprays.

6.2 Physical Interpretation. Helical instabilities of the type observed have been predicted theoretically (Mattingly and Chang 1974) and seen experimentally in both single-phase submerged jets and in two-phase liquid jets (Mattingly and Chang 1974; Hoyt and Taylor 1977). They stem from dynamic instabilities which are the result of momentum fluctuations and have wavelengths on the order of a few jet diameters. Theories which have been used to explain these phenomena are based on linearized equations of motion with an imposed perturbation of the form $\exp[in\phi + i\alpha (x-ct)]$, where x and ϕ are the longitudinal and the azimuthal cylindrical coordinates. When $n = 1$, the jet trajectory will become helical. If α is a complex number, the perturbation may grow exponentially with distance (i.e., spatial instabilities). The perturbations oscillate in both time and space. Our experimental results can be explained in terms of such spatial instability. Furthermore, the theories indicate that the helical instabilities ($n = 1$) dominate symmetric instabilities ($n = 0$) when the jet profile has more Gaussian than "top hat" character. This fits the observations that at higher ambient gas densities (test series A) the core becomes helical at shorter distances than at lower densities (test series B). For the same **global** gas density, the core transitions to a helical structure more rapidly when the ambient gas is hotter. This is probably due to higher **local** gas densities near the jet origin under these conditions. The helical trajectory pitch decreases with travel as the velocity decreases due to liquid momentum transfer to the ambient gas.

While helical instabilities develop in the core a few diameters from the origin, capillary instabilities associated with surface tension are responsible for the conically shaped spray envelope. These perturbations are axisymmetric (Reitz and Bracco 1986; Lin and Kang 1987) and dominate near the core origin. Such instabilities have wavelengths which are much smaller than the jet diameter. If, as a result, liquid droplets strip off the jet periphery, the liquid core is likely to decrease in diameter with distance from the origin until it becomes helical. Indeed, such behavior was observed in all tests except those conducted with ambient conditions above the critical point (series D and E).

The increase in the penetration distance with increase in pressure and temperature above the critical point can be explained if it is assumed that the core surface (including the surfaces of liquid blobs within the core) achieve critical temperatures within a short distance from the origin. In this case, the surface tension vanishes and the Ohnsorge number becomes very large. Indeed, theoretical predictions indicate that when the Ohnsorge number is large atomization is slow. Atomization is a relatively effective pathway for the transfer of momentum from the core to the ambient gas, and it increases the liquid surface area, facilitating evaporation. Slower atomization could produce the unexpectedly long axial core penetration observed in test series D and E.

The inward collapse of the annular jet core is presumably due to a low-pressure zone being established inside the annulus. The entrainment of the ambient gas by the inner-atomizing surface of the core could produce such a low-pressure zone. At higher gas densities, the entrainment is more effective and results in faster collapse. In high-temperature tests, it is probable that the gas inside the core has a lower temperature (and higher density) than the global environment. This would explain the jet collapse despite the low-global gas density (see, for example, Figure 6e.)

While the foregoing discussion provides interpretations for the observed trends, the scope of the analysis is limited. Other physical factors, such as the effect of the gas viscosity (which becomes higher with temperature) or additional processes related to thermal, mass, and momentum transfer at high pressures, may also be important.

7. PRACTICAL IMPLICATIONS

The experimental results show that the liquid core structure is affected by heat transfer at high pressures. The penetration of the core depends on ambient conditions in a manner not accounted for by present theories. Therefore, spray-combustion codes may give erroneous results. The experimental results indicate that the theories may underestimate the spray penetration at high pressures and temperatures. These observations have particular relevance to the high-intensity spray-combustion process in guns. Because core structures are inherently unstable and fluctuate with time, the fluctuations can trigger combustion noise that couples with acoustic modes in the chamber and result in pressure fluctuations. The situation may be aggravated if the pressure excursions periodically transit through critical levels. Pressure imbalances on the core of annular jets in guns may also result in combustion instabilities. However, this possibility requires further investigation. Gun-injector geometries are much more complex, with much thicker, higher-velocity jets than those observed in the present experimental study.

8. CONCLUSIONS

- Flash x-ray radiography has been successfully employed to resolve small (0.1 mm) details in the cores of evaporating CH_3I jets at elevated pressures and temperatures.

- It was observed that the core structure is strongly affected by heat transfer.

- The core structure is inherently unstable, forming helical structures whose wavelengths are larger than the jet diameter.

- The penetration of all cores decrease with ambient gas density. For the same gas density, the lengths of evaporating cores decrease with pressure, reach a minimum at some critical pressure, then increase with further rise in pressure. The minimum corresponds to a transition to a temperature and pressure regime above the thermodynamic critical point of the liquid.

- The results indicate that core fluctuations are a potential source of instability in combusting sprays.

INTENTIONALLY LEFT BLANK.

9. REFERENCES

Baev, V. K., A. N. Bazhaikin, A. A. Buzukov, B. P. Timoshenko, E. I. Bichenko, and R. L. Rabinovich. "Experimental Study of the Development and Structure of High-Velocity Liquid Jets in Air." Prog. Astronautics and Aeronautics, vol. 105, p. 104, 1986.

Birk, A., and P. Reeves. "Annular Liquid Propellant Jets - Injection, Atomization, and Ignition." BRL-TR-2780, U.S. Army Ballistic Research Laboratory, Aberdeen Proving Ground, MD, March 1987.

Birk, A., and M. McQuaid. "A Particle Bed Heater for Creating a Clear, High-Pressure Gas Flow." Rev. Sci. Instr., vol. 64, p. 2673, September 1993.

Birk, A., M. McQuaid, and G. Bliesener. "Reacting Liquid Monopropellant Sprays- Experiments With High Velocity Full Cone Sprays in 33 MPa, 500 C Nitrogen." ARL-TR-17, U.S. Army Research Laboratory, Aberdeen Proving Ground, MD, December 1992.

Chehroudi, B., S. H. Chen, F. V. Bracco, and Y. Onuma. "On the Intact Core of Full-Cone Sprays." SAE Paper 850126, 1985.

Freedman, E. "BLAKE - A Thermodynamics Code Based on TIGER: Users' Guide and Manual." BRL-TR-02411, U.S. Army Ballistic Research Laboratory, Aberdeen Proving Ground, MD, July 1982.

Gonzalez, M. A., and R. D. Reitz. "Modeling Diesel Engine Spray Vaporization and Combustion." Proceedings of the 5th International Conference on Liquid Atomization and Spray Systems, 1991.

Hewlett-Packard, Inc. "Flash Radiography - Simultaneous High Contrast and Penetration." Technical Bulletin B-23, 1973.

Hoyt, J. W., and J. J. Taylor. "Waves on Water Jets." Journal of Fluid Mechanics, vol. 83, p. 119, 1977.

Krehl, P., and D. Warken. "Flash Soft Radiography - Its Adaption to the Study of Breakup Mechanisms of Liquid Jets into a High-Density Gas." Proceedings of the 19th International Congress on High-Speed Photography and Photonics, September 1990.

Lin, S. P., and D. J. Kang. "Atomization of a Liquid Jet." Physics of Fluids, vol. 30, p. 2000, July 1987.

Mattingly, G. E., and C. C. Chang. "Unstable Waves on an Axisymmetric Jet Column." Journal of Fluid Mechanics, vol. 65, 1974.

Morrison, W. F., J. D. Knapton, and M. J. Bulman. "Liquid Propellant Guns." Gun Propulsion Technology, vol. 109, Prog. in Astronautics and Aeronautics, 1988.

Reitz, R. D., and F. V. Bracco. "Mechanisms of Breakup of Round Liquid Jets." Encyclopedia of Fluid Mechanics, 1986.

Warken, D., and P. Krehl. "Application of Flash Radiography to the Analysis of Simulated Liquid Gun Propellant Jets." Proceedings of the 12th International Symposium on Ballistics, October 1990.

INTENTIONALLY LEFT BLANK.

NO. OF COPIES	ORGANIZATION
2	DEFENSE TECHNICAL INFO CTR ATTN DTIC DDA 8725 JOHN J KINGMAN RD STE 0944 FT BELVOIR VA 22060-6218
1	DIRECTOR US ARMY RESEARCH LAB ATTN AMSRL OP SD TA 2800 POWDER MILL RD ADELPHI MD 20783-1145
3	DIRECTOR US ARMY RESEARCH LAB ATTN AMSRL OP SD TL 2800 POWDER MILL RD ADELPHI MD 20783-1145
1	DIRECTOR US ARMY RESEARCH LAB ATTN AMSRL OP SD TP 2800 POWDER MILL RD ADELPHI MD 20783-1145
	ABERDEEN PROVING GROUND
5	DIR USARL ATTN AMSRL OP AP L (305)

NO. OF COPIES	ORGANIZATION
1	COMMANDER US ARMY ARDEC ATTN SMCAR AEE B D DOWNS PICATINNY ARSENAL NJ 07805-5000
2	COMMANDER US ARMY ARDEC ATTN SMCAR AEE BR B BRODMAN W SEALS PICATINNY ARSENAL NJ 07806-5000
1	COMMANDER US ARMY ARDEC ATTN SMCAR AEE W N SLAGG PICATINNY ARSENAL NJ 07806-5000
2	COMMANDER US ARMY ARDEC ATTN SMCAR AEE A BRACUTI D CHIU PICATINNY ARSENAL NJ 07806-5000
4	COMMANDER ATTN SMCAR FSS DA B MACHAK S TRAENDLY C PERAZZO R KOPMAN BLDG 94 PICATINNY ARSENAL NJ 07806-5000
2	COMMANDER ATTN SFAE ASM AF A LTC D ELLIS J SHIELDS BLDG 3159 PICATINNY ARSENAL NJ 07806-5000
1	COMMANDANT US ARMY ARMOR CTR ATTN ATSB CD MLD FT KNOX KY 40121
1	COMMANDANT USAFAS ATTN ATSF TSM CN FT SILL OK 78503-5600

NO. OF COPIES	ORGANIZATION
1	COMMANDER HS AMCCOM ATTN AMSMC LSL B KELEBER ROCK ISLAND IL 61299-6000
1	COMMANDER HS AMCCOM ATTN AMSMC SAS WF G SCHELENKER ROCK ISLAND IL 61299-6000
1	DIRECTOR ATTN AMXRO MCS DR D MANN PO BOX 12211 RESEARCH TRIANGLE PARK NC 27709-2211
1	DIRECTOR ATTN AMXRO RT IP LIB SER PO BOX 12211 RESEARCH TRIANGLE PARK NC 22709-2211
1	OLAC PL RKFA ATTN D TALLEY EDWARDS AFB CA 93524
1	CA INST OF TECHNOLOGY JET PROPULSION LAB ATTN TECHNICAL LIBRARY 4800 OAK GROVE DR PASADENA CA 91109-8099
1	THE PENN STATE UNIV ATTN PROF K KUO 140 RESEARCH BLDG E BIGLER RD UNIVERSITY PARK PA 16802-7501
2	DIRECTOR JET PROPULSION LAB ATTN D P MAYNARD J BELLAN 4800 OAK GROVE DR PASADENA CA 91109-8099
1	VEHICLE PROPULSION DIRECTORATE NASA LEWIS RESEARCH CTR ATTN MS 603 TECH LIB 21000 BROOKPARK RD CLEVELAND OH 44135-3191

NO. OF COPIES	ORGANIZATION
1	DIRECTOR SANDIA NATL LABS ATTN R CARLING DIV 8357 PO BOX 696 LIVERMORE CA 94551-0969
1	DIRECTOR THE JOHNS HOPKINS UNIV ATTN APPLIED PHYSICS LAB JOHNS HOPKINS RD LAUREL MD 20707
1	PAUL GOUGH ASSOC INC ATTN DR P GOUGH 1048 SOUTH ST PORTSMOUTH NH 03801-5423
2	JOHNS HOPKINS UNIV CPIA ATTN T CHRISTIAN TECHNICAL LIBRARY 10630 LITTLE PATUXENT PKWY STE 202 COLUMBIA MD 21042-3200

NO. OF COPIES	ORGANIZATION
	ABERDEEN PROVING GROUND
39	DIR, USARL ATTN: AMSRL-WT-P, A. HORST AMSRL-WT-PA, T. MINOR T. COFFEE G. WREN A. BIRK (10 CPS) J. DE SPIRITO A. JUHASZ J. KNAPTON C. LEVERITT M. MCQUAID (5 CPS) B. OBERLE P. TRAN K. WHITE L-M. CHANG J. COLBURN P. CONROY G. KELLER D. KOOKER M. NUSCA T. ROSENBERGER AMSRL-WT-PB, E. SCHMIDT AMSRL-WT-PC, R. FIFER J. VANDERHOFF R. BEYER M. MILLER AMSRL-WT-PD, B. BURNS

INTENTIONALLY LEFT BLANK.

USER EVALUATION SHEET/CHANGE OF ADDRESS

This Laboratory undertakes a continuing effort to improve the quality of the reports it publishes. Your comments/answers to the items/questions below will aid us in our efforts.

1. ARL Report Number ARL-TR-901 Date of Report December 1995

2. Date Report Received _____

3. Does this report satisfy a need? (Comment on purpose, related project, or other area of interest for which the report will be used.) _____

4. Specifically, how is the report being used? (Information source, design data, procedure, source of ideas, etc.) _____

5. Has the information in this report led to any quantitative savings as far as man-hours or dollars saved, operating costs avoided, or efficiencies achieved, etc? If so, please elaborate. _____

6. General Comments. What do you think should be changed to improve future reports? (Indicate changes to organization, technical content, format, etc.) _____

CURRENT ADDRESS

_____
Organization

_____
Name

_____
Street or P.O. Box No.

_____
City, State, Zip Code

7. If indicating a Change of Address or Address Correction, please provide the Current or Correct address above and the Old or Incorrect address below.

OLD ADDRESS

_____
Organization

_____
Name

_____
Street or P.O. Box No.

_____
City, State, Zip Code

(Remove this sheet, fold as indicated, tape closed, and mail.)
(DO NOT STAPLE)

DEPARTMENT OF THE ARMY

OFFICIAL BUSINESS

NO POSTAGE
NECESSARY
IF MAILED
IN THE
UNITED STATES

BUSINESS REPLY MAIL
FIRST CLASS PERMIT NO 0001,APG,MD

POSTAGE WILL BE PAID BY ADDRESSEE

DIRECTOR
U.S. ARMY RESEARCH LABORATORY
ATTN: AMSRL-WT-PA
ABERDEEN PROVING GROUND, MD 21005-5066